Renewable Energy 141 (2019) 516–525

Contents lists available at ScienceDirect

Renewable Energy

journal homepage: www.elsevier.com/locate/renene

Investigation of semi-transparent dye-sensitized solar cells for fenestration integration

Prabhakaran Selvaraj*, Aritra Ghosh, Tapas K. Mallick, Senthilarasu Sundaram*

Environment and Sustainability Institute (ESI), University of Exeter, Penryn Campus, TR10 9FE, United Kingdom

ARTICLE INFO

Article history:
Received 9 October 2018
Received in revised form
2 February 2019
Accepted 31 March 2019
Available online 3 April 2019

Keywords:
DSSC
Glazing
Solar factor
Angular transmission
Clearness index
Daylight glare

ABSTRACT

For any particular location glazing transmission varies with season and time of day. Thus, glazing transmission angular behaviour is more crucial than single glazing transmittance value for building energy simulation and design. In this work, the spectral behaviour of the dye-sensitized solar cell (DSSC) glazing with three different transparencies are studied. Transmittance of the devices are measured after 2 years to understand the effects of device stability on DSSC glazing applications. The solar factor for the devices is calculated for different light incident angles for a whole year at a particular location. The correlation between clearness index and DSSC transmittance is also studied. Finally, glare analysis is performed for all the devices on a sunny day, intermittent day and overcast day, and is also compared with double glazing. It is found that the 37% transparent DSSC glazing leads to a greater reduction in disturbing glare by 21% compared to double glazing on a clear sunny day. All the above results suggest that DSSC glazings could be productively used for fenestration integration in buildings.

1. Introduction

According to the world energy report, buildings consume 34% of world energy demand and are responsible for 6% of greenhouse gas emission [1]. The building sector in the U.S accounts for about 39% of total energy consumption for heating, ventilation, cooling and lighting load demand [2]. It is projected that energy-related GHG emissions will rise about 14% by 2035 [3]. To follow the aim of the Paris agreement, reduction of GHG emission is essential to keep the global warming well below 2 °C [4]. Thus, it is important to have energy efficient buildings in order to protect the environment from the adverse effects of these emissions.

Buildings are composed of different envelopes such as doors, roofs, walls and windows. Due to the transparent nature of a window, it has a large impact on the energy demand as well as the thermal and visual comfort of a building [5,6]. Presently available single or double glazed windows allow a considerable amount of solar heat for hot climates and excessive heat loss for cold climates, also daylight which creates glare [7,8]. On the other hand, smart or advanced type glazings have the potential to reduce building energy demand. Switchable and static transparent type of advanced glazings are currently available [9]. Static transparent PV glazings are promising for window applications due to their multifunctional property such as ability to control solar gain, daylight glare and generate clean electricity [10,11]. PV glazings are also known as BIPV glazing because it replaces buildings traditional windows and becomes an integral part of the building. BIPV can also replace other building envelopes such as walls and roof. However, the windows of a building are of prime importance as it is the only building envelope which maintains a relation between external environment and internal room [9]. Thus, advanced BIPV windows are required to allow soothing daylight and also to control the solar heat by using a single system.

For glazing application, semitransparency is a precondition [12]. Natural daylight penetrating through this semi-transparent PV makes the indoor environment comfortable. Available PV types for glazing application include crystalline silicon, CdTe, a-Si, CIGS, DSSC and perovskite. c-Si has higher absorption which restricts light to pass through. There are many studies in the literature where c-Si PV was used to replace traditional glazing at homes or buildings. Since these cells are typically opaque, there are also important compromises in terms of lighting (shadows in the building interior) and limited external view [13–16]. The need to increase the natural light transmission without reducing the PV efficiency directed to the study of lighter and see through thin film PV. Regular distribution of opaque c-Si can offer daylighting, however this structure blocks the natural viewing [11]. Thin film second generation CdTe

* Corresponding authors.
E-mail addresses: ps364@exeter.ac.uk (P. Selvaraj), s.sundaram@exeter.ac.uk (S. Sundaram).

https://doi.org/10.1016/j.renene.2019.03.146

Nomenclature

E_v	Vertical illuminance (lux)
k	Extinction coefficient
d	Diffuse fraction of total solar radiation
g	Solar factor/solar heat gain coefficient
k_T	Clearness index
n	Refractive index
r_b	Ratio of the beam radiation on an inclined surface to that on a horizontal surface
q_i	Infrared radiation
h_e	External heat transfer coefficient
h_i	Internal heat transfer coefficient
SR	Subjective rating

Greek symbols

α	Absorptance
ρ	Reflectance
ρ_s	Solar reflectance
ρ_g	Ground solar reflectance
τ_s	Solar transmittance
τ_{dir}	Direct transmittance
τ_{diff}	Diffuse transmittance

[17], a-Si [18] and CIGS [19] are other options for PV glazing application. With thin film incorporation in a glass–glass construction, commercial products with a transparency up to 50% are available in the market. The introduction of this technology provided more homogeneous daylighting of the interior spaces compared to crystalline solar cells. However, light induced defects, shortage and toxicity of materials used in a-Si, CIGS, and CdTe technologies have limited the opportunity to apply them in glazing application [20]. Moreover, the power conversion efficiency is connected to its visual transmittance and therefore extensive performance optimization should be considered [21–23].

Third generation DSSC is a potential candidate for BIPV applications due to its low manufacturing cost [24], semi-transparent nature to transmit soothing daylight, short payback time and positive temperature coefficient [25]. Fig. 1 shows the schematic architecture of DSSC glazing. Previously, fabricated DSSC module using 9 unit cells ($0.8 \times 0.8\ cm^2$) in a series connection offered 60% transmission in the wavelength range between 500 and 900 nm [26]. Thermo-optical behaviour of DSSCs made of green and red dyes were investigated using WINDOW software, which showed 60% reduction of solar gain [27]. Thermo-opto-electrical characteristics of DSSC were investigated by Zemax, WINDOW and COMSOL softwares [28]. To evaluate the occupant comfort due to the colour property of transmitted solar light, correlated colour temperature and colour rendering index for DSSC glazing was evaluated [29]. Recently, DSSC glazing was monitored for two years in outdoor exposure at Hanbat National University, Republic of Korea (36.20° N, 127.18° E), which showed promising outcomes [30]. Another outdoor experiment was also performed to study the thermal performance for DSSC glazing which showed overall heat transfer coefficient and solar heat gain coefficient for this glazing were 3.6 W/m2K and 0.2 respectively [31].

For glazing, transmission is a dominant parameter which is not constant but varies with solar incident angle. The incident angle of sunlight varies with the time of day and season. Therefore, building integrated vertical plane DSSC glazing's transmission is significantly different from their normal incidence value. For building energy simulation, this variable transmission evaluation is essential to predict accurate energy saving calculation. Glazing transmittance also has a strong correlation with clearness index, and knowing this value helps in building energy calculation. To evaluate clearness index, the only measured parameter is global horizontal solar radiation. As DSSC is considered to be in wide future as one of the future PV glazing materials, its angular transmission behaviour variation with clearness index evaluation is essential.

In this work, clearness index and glazing transmission correlation was evaluated. To understand the potential glare control saving using DSSC glazing, subjective glare analysis was performed using measured external illuminance and the results were compared with a double glazing. According to the authors' knowledge, this is the first report on glare analysis of DSSC, correlation between DSSC glazing transmission with incident angle and clearness index.

2. Experimental method

2.1. DSSC fabrication

Transparent dye-sensitized solar cells were prepared according to the literature procedures [32,33]. Nanocrystalline transparent

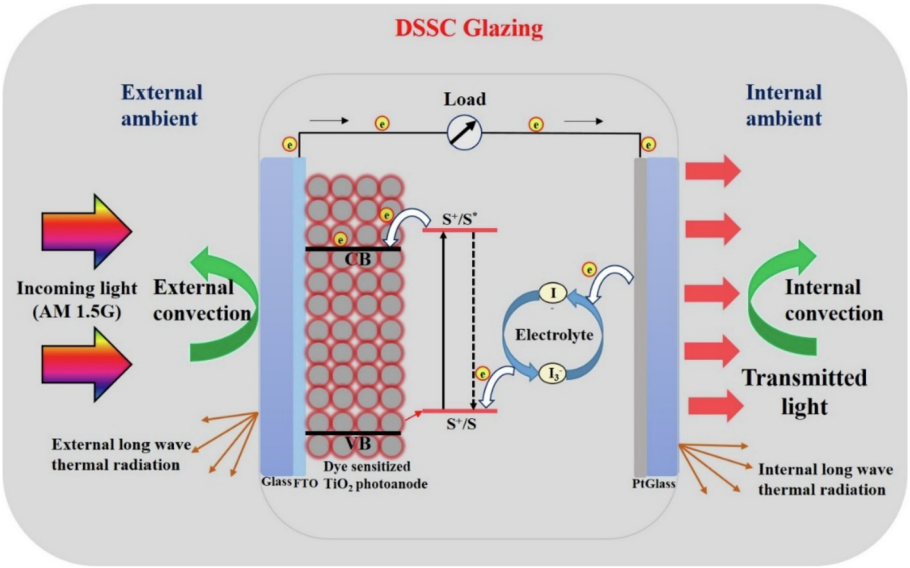

Fig. 1. Schematic representation of DSSC glazing.

TiO_2 films of different thicknesses were deposited onto transparent conducting glass (fluorine-doped tin oxide layer, sheet resistance of 13 Ω/cm^2). The thickness of the TiO_2 electrodes (Table 1) was measured using Dektak 8 Advanced Development Profiler. The TiO_2 electrodes were soaked overnight in an ethanolic solution of 1×10^{-6} M N719 dye (Solaronix SA), sandwiched with a platinised conducting counter electrode using a Surlyn frame (Solaronix SA) in between, filled with the iodide/tri-iodide liquid electrolyte through a hole in the counter electrode and sealed.

2.2. DSSC characterisation

The optical properties of the fabricated DSSCs was measured using a UV-VIS-NIR spectrometer (PerkinElmer, Lambda 1050). Fig. 2 represents the optical measurement method of the devices. The photovoltaic performance parameters of the devices were measured using an indoor continuous solar simulator (Wacom AAA; model: WXS-210S-20; 1000 W/m^2, AM1.5G). All the transparent solar cells were kept in a dark box for 2 years and the optical measurements were carried out again for comparison.

Previously, we fabricated DSSCs with different transparencies from 53% to 19% and studied their indoor photovoltaic performance. It was found that, the photovoltaic performance of the DSSCs increases with a decrease in device transparency, before it starts decreasing for the low transparent devices. The DSSC with 37% transparency in the visible range produced about 6% power conversion efficiency. The same device was scaled up to understand the potential of DSSCs in building applications. Solar concentrators were also coupled with the devices and it was found that the low solar concentrators could improve the efficiency of the transparent DSSCs. The impact of temperature on PV performance was also analysed.

In our next investigation, the correlated colour temperature (CCT) and colour rendering index (CRI) for DSSC glazing application were calculated. After comparing the results, it was found that the transparent DSSCs offer only 2.7% lower CRI and CCT values than the vacuum and double-glazing. All the above results have been reported [29,33,34]. Fig. 3 compares the electrical efficiency and CRI of the devices with their transparencies. It has been found that the devices with higher transparency have better CRI and CCT values. Since L5 device has the highest efficiency among all with 37% transparency and devices L2 and L3 are aesthetically suitable, we consider these three devices named as L2, L3 and L5 with 53%, 50% and 37% transparency respectively for further analysis in this work.

Table 1
Various DSSCs fabricated and their optical and electrical performance parameters.

Device name	TiO_2 thickness (μm)	Transparency (%)	Power conversion efficiency (%)
L2	3.5	53	2.51
L3	6	50	4.49
L4	8	44	5.02
L5	10	37	5.93
L6	12	25	5.15
L7	14	19	3.24

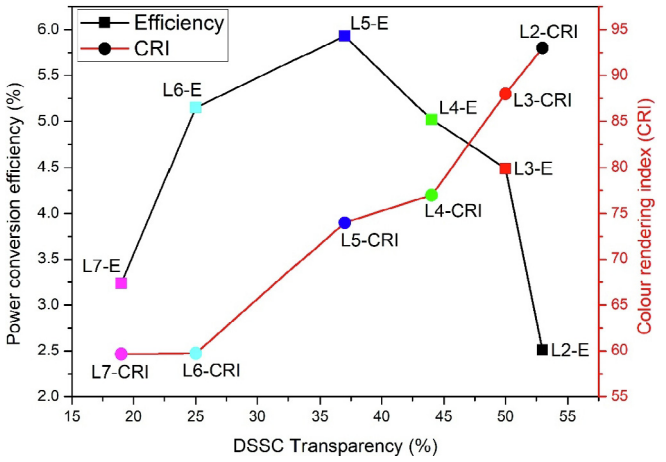

Fig. 3. Comparison of electrical efficiency and CRI for DSSCs with different transparencies.

3. Methodology

3.1. Angular transmission

Angular dependent glazing transmission is given by Refs. [35,36].

$$\tau_s(\theta) = \frac{1}{2}\left[\frac{1-\left\{\frac{\sin(\theta-n)}{\sin(\theta+n)}\right\}^2}{1+(2n_g-1)\left\{\frac{\sin(\theta-n)}{\sin(\theta+n)}\right\}} + \frac{1-\left\{\frac{\tan(\theta-n)}{\tan(\theta+n)}\right\}^2}{1+(2n_g-1)\left[\frac{\tan(\theta-n)}{\tan(\theta+n)}\right]^2}\right] \times \exp\left(\frac{-k_g N_g t_g}{\cos\theta}\right) \quad (1)$$

Where extinction coefficient (k) and refractive index (n) can be found from equations (2) and (3) respectively

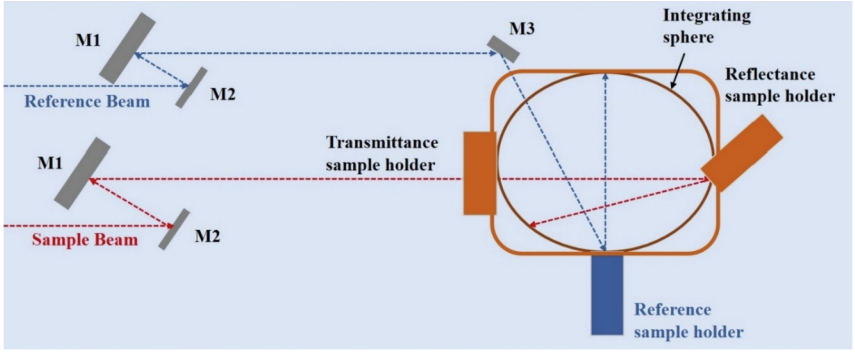

Fig. 2. Schematic representation of the UV/vis/NIR spectrophotometer used for optical measurements.

$$k = -\frac{\lambda}{4\pi d}\ln t \tag{2}$$

$$n = \frac{(1+\sqrt{r})}{(1-\sqrt{r})} \tag{3}$$

Internal radiometric properties r and t are defined as follows

$$r = \frac{\beta - \sqrt{\beta^2 - 4(2-\rho)\rho}}{2(2-\rho)} \tag{4}$$

$$t = \frac{(\rho - r)}{r\tau_s} \tag{5}$$

3.2. Solar factor

The solar factor or solar heat gain coefficient of a glazing indicates the fraction of the entering incident solar radiation into a room after passing through that glazing material [37]. It also measures the transmitted solar energy through a glazing. This is the sum of the solar transmittance (τ_s) and entering infrared radiation (q_i) to a building interior [38]. Angular dependent solar transmission from equation (1) is replaced in equation (6).

$$\begin{aligned} g &= \tau_s + q_i = \tau_s + \alpha\frac{h_i}{h_i + h_e} \\ &= \tau_s + (1 - \tau_s - \rho_s)\frac{h_i}{h_i + h_e} \end{aligned} \tag{6}$$

Angular solar factor (g(θ)) was evaluated using equation (7)

$$g(\theta) = g(0)\tau_s(\theta) \tag{7}$$

3.3. Glazing transmission and clearness index

The relationship between clearness index and glazing transmittance is given by equation (8) [35].

$$\begin{aligned} \tau = \tau_0 &\left\{ d[k_T r_b(1-d) + (1-\cos\theta)(1-k_T(1-d))] + r_b(1-d) + \rho_g\frac{(1-\cos\beta)}{2} \right\} \times \\ &\left\{ \frac{\tau_{dir}}{\tau_0} r_b(1-d)(1+k_T d) + \frac{\tau_{diff}}{\tau_0}\frac{d}{2}(1+\cos\theta)(1-k_T(1-d)) + \frac{\tau_g}{\tau_0}\frac{\rho_g(1-\cos\theta)}{2} \right\} \end{aligned} \tag{8}$$

From equation (1) $\tau = \tau_{dir}$ when $\theta = \theta_{dir}$.

$\tau = \tau_{dif}$ *When* $\theta = \theta_{dif} = 59.68 - 0.1388\beta + 0.001497\beta^2$ [39].

$\tau = \tau_g$ *When* $\theta = \theta_g = 90 - 0.5788\beta + 0.002693\beta^2$ [39].

(Ground reflection (ρ_g) was considered as 0.2 and used in the calculations).

3.4. Glare analysis

To identify the daylight glare control potential of these DSSC glazings, theoretical analysis using measured outdoor vertical illuminance was employed. Glare index calculation is provided for a DSSC glazing for a typical sunny day, intermittent day and overcast day in Penryn, UK (50.16° N, 5.10° W). The DSSC glazing is considered to be on a vertical south façade. The dimensions of the glazing were considered as 30 × 30 × 0.5 (l × w × h) cm in the scale model. The dimensions of the room, glazing position and measuring points are shown in Fig. 4. These dimensions resemble the DSSC as a large glazed façade, while the internal surface of the unfurnished room has white paint (0.8 reflectance) as mentioned previously [40]. The glare subjective rating is [41] given by equation (9) where E_V is the vertical illuminance facing the window (worst case) measured at the centre of the room. This SR index allows discomfort glare estimation experienced by subjects when working at a visual daylight task (VDT) placed against a window of high or not uniform luminance. The reason for selecting this index is the engagement of only one photo sensor which can save time and cost. The criterion scale of discomfort glare subjective rating is given in Table 2. This method also allows the non-intrusive measuring equipment necessary for scale model daylighting assessments [42,43].

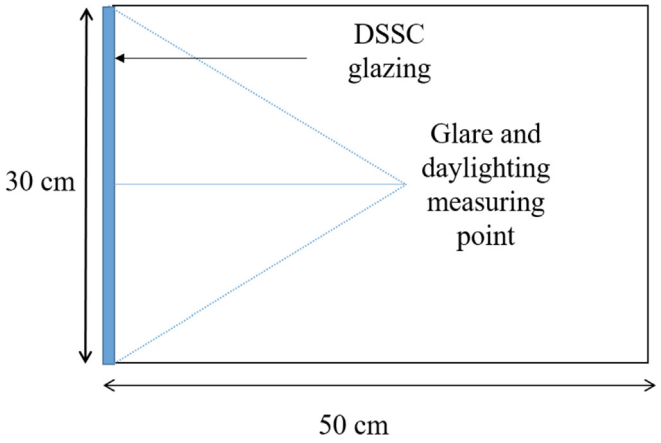

Fig. 4. Schematic cross section of a room with DSSC glazing place on vertical south facade.

$$SR = 0.1909E_v^{0.31} \tag{9}$$

Table 2
Criterion scale of discomfort glare subjective rating (SR) [41].

Comfort level indicator	Glare subjective rating (SR)
Just intolerable	2.5
Just disturbing	1.5
Just noticeable/accepting	0.5

4. Results and discussion

4.1. Spectral behaviour of the devices

Fig. 5 shows transmission, reflection and absorption curves for L2, L3 and L5 devices. Average transmission for L2, L3, L5 are 53%, 50%, 37% and reflections are 40% 44% and 53% respectively. For comparison, the product of relative spectral distribution of illuminant D65 (Dλ) and the spectral luminous efficiency for photopic vision, V(λ) is the photopic luminous efficiency function of the human eye and has also been added which ranges from 400 to 700 nm with its peak at 555 nm. This type of DSSC glazing has low NIR transmission after 1600 nm and high visible transmission which is promising for glazing application. Peak transmission occurs around 750 nm for all the devices. Below 400 nm and above 700 nm, the product DλV(λ) is zero since V(λ) is zero. Beyond 700 nm, the optical performance of all the DSSCs is similar. Fig. 5 compares the optical performance of the devices with the photopic eye sensitivity to light wavelength.

As DSSCs have long term stability issues, the optical properties of the devices were measured after two years. Fig. 6 compares the transmittance of both fresh and old devices. The transparency of

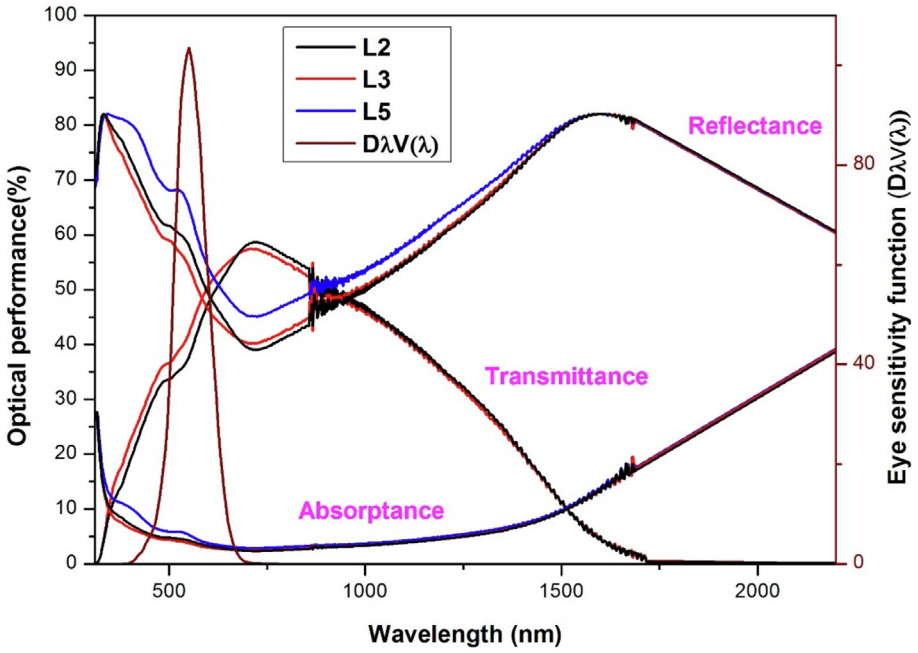

Fig. 5. Optical performance of the transparent DSSCs.

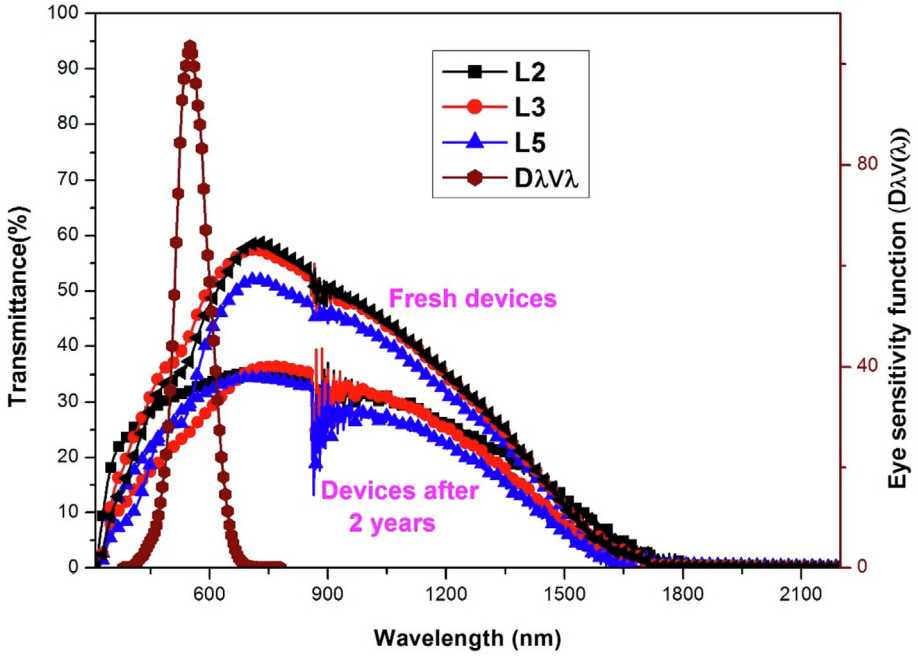

Fig. 6. Comparison of transmittance of the different transparent DSSCs (Fresh and after 2 years).

the devices is decreased by 20–30% after 2 years compared to the initial measurement. This could be due to the interfacial reaction in the device. Since the electrolyte has corrosive characteristics, corrosion of the electrode in the electrolyte solution frequently occurs resulting in poor transparency of the cell. Though the electrodes are corroded, the devices still transmit the light. For glazing perspective, the durability based on transmission is comparable with other smart glazing [44].

4.2. Solar factor

Spectral transmittance and reflectance at normal incidence are the most commonly measured optical properties of glazing. For vertical plane DSSC glazing, transmission varies with light incident angle. Here, using equation (1), incident angle dependent glazing's angular transmission was calculated from measured normal incident transmission. Fig. 7 shows the angular dependency of the L2,

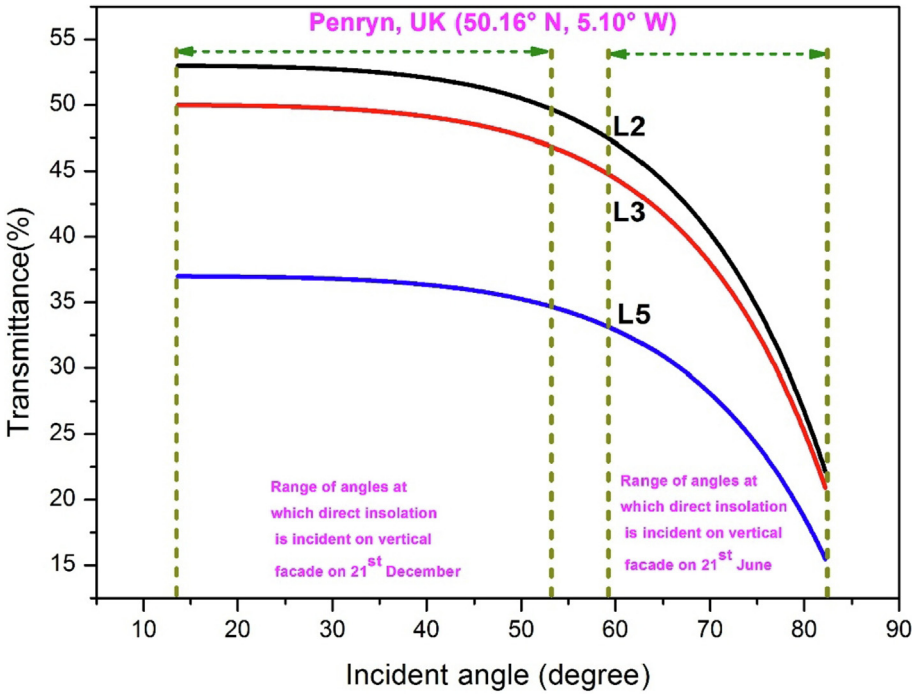

Fig. 7. Variation of DSSC transmission with solar incident angle.

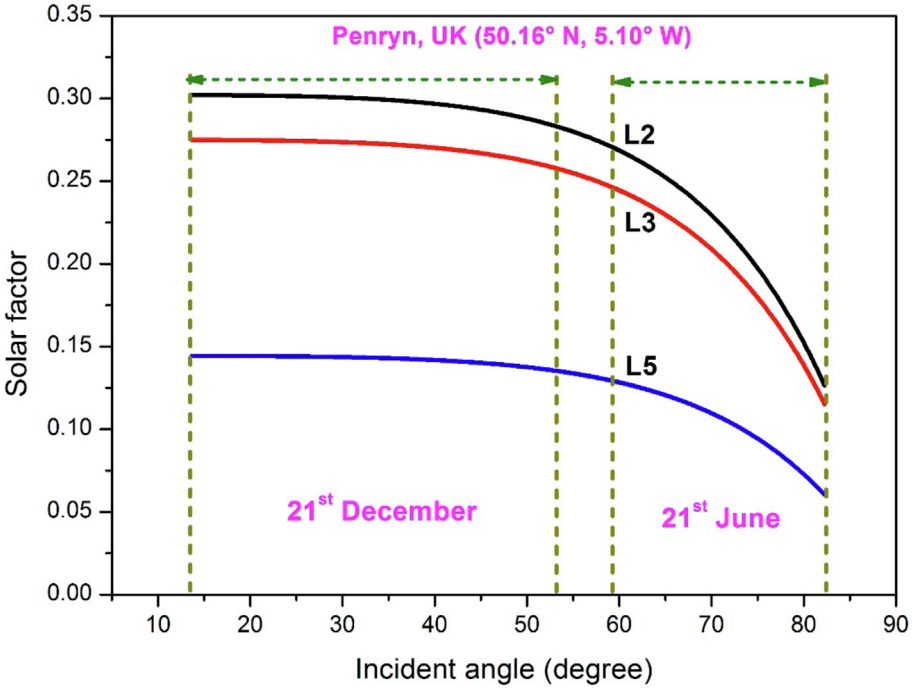

Fig. 8. Variation solar factor with solar incident angle.

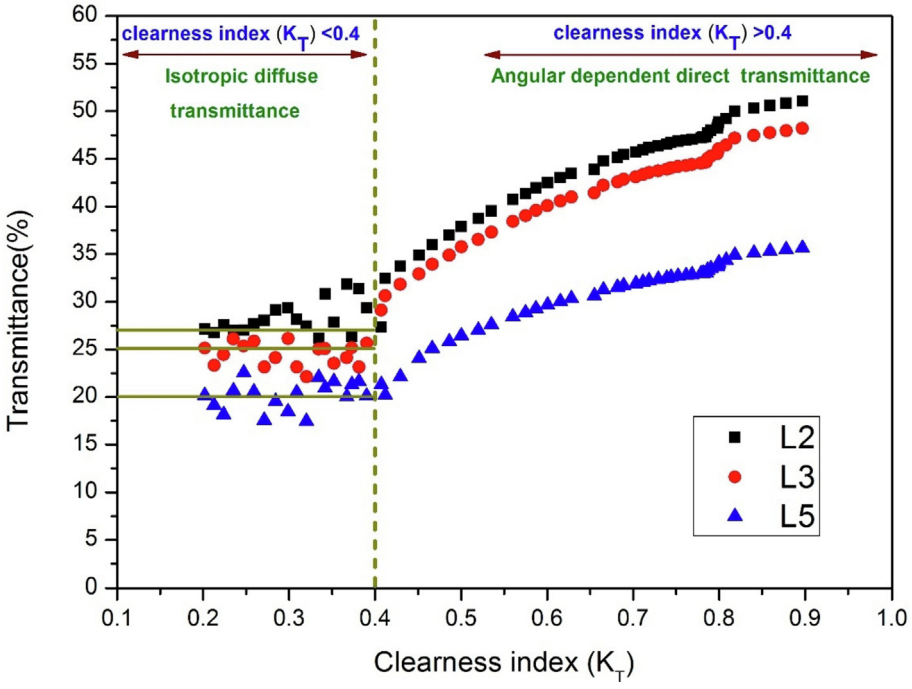

Fig. 9. Variation of DSSC transmission with clearness index.

Table 3
Yearly useable single transmittance value of DSSCs for different transparency, different azimuthal and monthly clearness index.

Inclination	Azimuthal orientation	Mean monthly clearness index	Transmittance		
			L2 DSSC	L3 DSSC	L5 DSSC
Vertical plane DSSC	North	0.7	27%	25%	20%
	South	0.4	27%	25%	20%
	East, West, North West, North East	0.6	27%	25%	20%

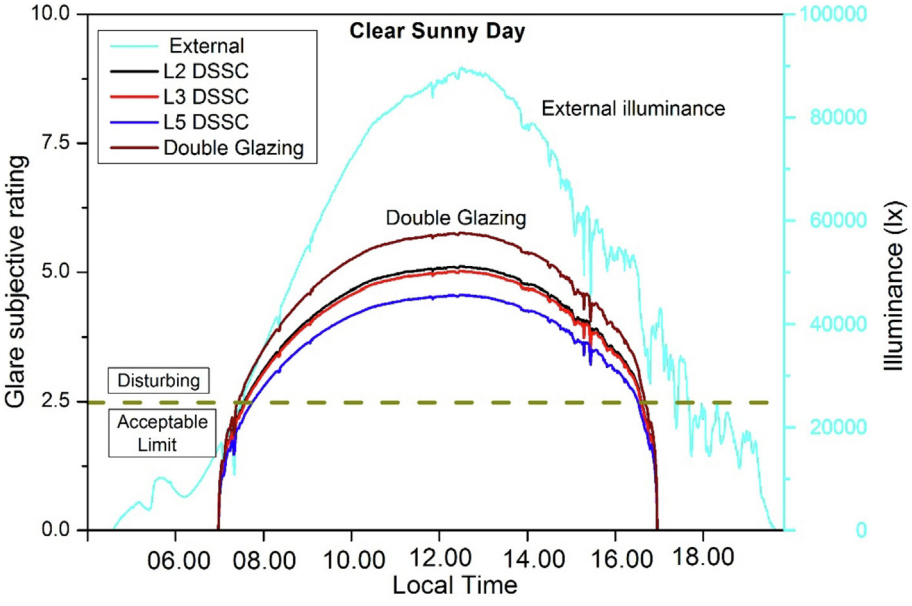

Fig. 10. Daylight glare index of transparent DSSC and double glazing for a typical clear sunny day at Penryn, University of Exeter.

L3 and L5 DSSC glazing devices. For the University of Exeter in Penryn, the incident angle varies from 13° to 82° throughout the year. For the month of December, glazing transmission is high compared to month of June.

As both conductive glasses are sealed in DSSC, little air gap is present between the two glass panes. So, the whole device was considered as a single glazing (4.4 mm thickness). Using equation (7), angular solar factor was calculated and shown in Fig. 8. External heat transfer coefficient (h_e) of 25 W/m^{2}K, internal heat transfer coefficient (h_i) of 7.7 W/m^{2}K, and wind speed of 4 m/s were considered to evaluate the solar factor for the normal incident angle. L2, L3 and L5 DSSC glazings have solar factors of 0.57, 0.55 and 0.39 respectively at normal incidence angle. However, due to the angular transmission, this solar heat gain is not achievable in DSSC glazing [45].

4.3. Variation of transmission with clearness index

The correlation between clearness index and glazing transmittance was evaluated for DSSC glazing and shown in Fig. 9. Isotropic diffuse transmittance is dominant for clearness index below 0.4, whereas angular dependent direct transmission is dominant after 0.4. For vertical plane DSSC glazing, transmittance varies with season, day and time. However, for south facing vertical plane DSSC glazing, single value glazing transmittance of 20% for L5, 25% for L3 and 27% for L2 can be chosen throughout the year while clearness index is less than 0.5. This study offers a yearly useable single glazing transmittance for DSSC glazing, which is

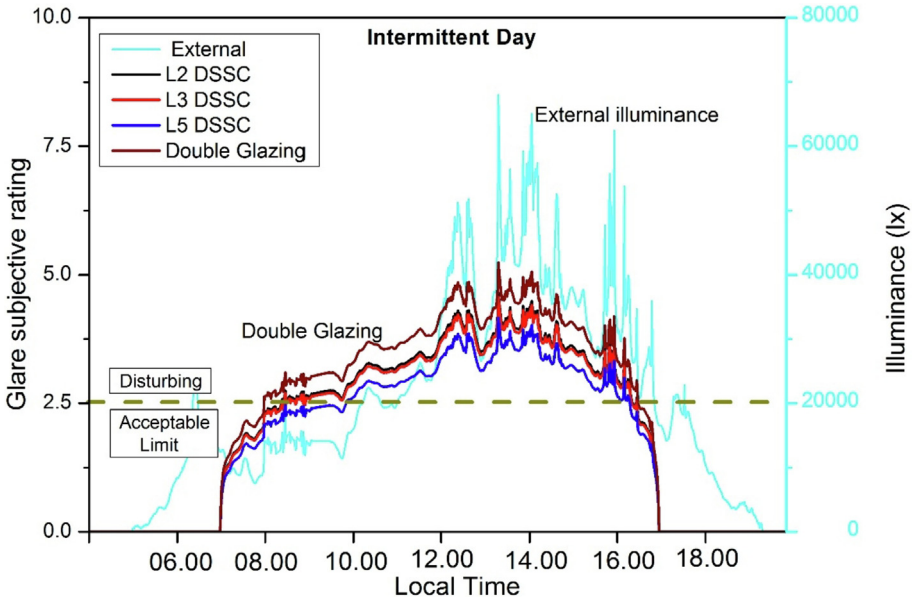

Fig. 11. Daylight glare index of transparent DSSC and double glazing for an intermittent day at Penryn, University of Exeter.

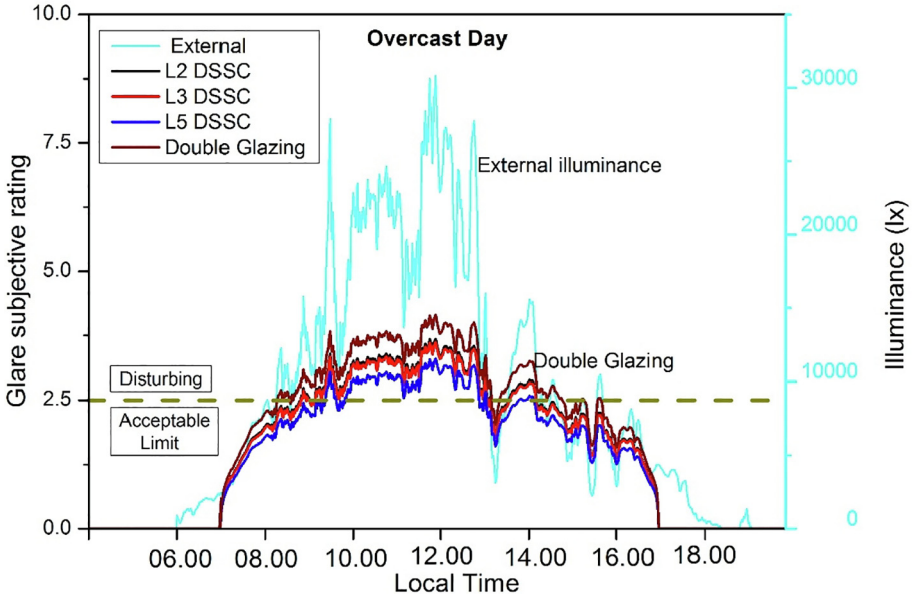

Fig. 12. Daylight glare index of transparent DSSC and double glazing for a typical cloudy day at Penryn, University of Exeter.

Table 4
Comparison of glare subjective ratings for a typical sunny, intermittent cloudy and overcast day for different glazing types at mid-day.

Weather	Glare subjective rating (SR) @ mid-day			
	Double Glazing	L2 DSSC	L3 DSSC	L5 DSSC
Clear sunny day	5.70	5.10	4.95	4.50
Intermittent cloudy day	4.30	3.75	3.70	3.40
Overcast day	3.80	3.40	3.35	3.10

advantageous for the building designers in northern latitude areas. For others, azimuthal orientation single achievable glazing transmission below the threshold clearness index is listed in Table 3.

4.4. Daylight glare analysis

Glare analysis was performed using equation (8). Wavelength dependent spectrum data for double glazing was collected from Ref. [8]. Illuminance data was recorded for south facing vertical plane on the roof of the ESI building in Penryn, UK (50.16° N, 5.10° W) using the illuminance sensor from MESA. Fig. 10, Fig. 11 and Fig. 12 show the daylight control potential using three different transparent DSSCs and a double glazing for a typical clear sunny day (0–5% opaque cloud coverage), intermittent cloudy day (26–50% opaque cloud coverage) and overcast day (88–100% opaque cloud coverage) respectively. Around mid-day, all types of glazings allowed an excessive amount of light which creates disturbing glare on a clear sunny day. Despite this, all the glazings allow excessive light which creates disturbing glare, 21% reduction in glare subjective rating is observed for the 37% transparent DSSC glazing compared to double glazing on a clear sunny day. During peak hours (mid-day) glare reduction is less in all the DSSC glazings for intermittent cloudy and overcast days as well. The glare subjective rating for a typical sunny, intermittent cloudy and overcast day for different glazing types are compared in Table 4.

5. Conclusions

Suitability of semi-transparent dye-sensitized solar cells (DSSC) for fenestration integration was investigated in this work. To obtain this, three different transparency (named in this work as L2, L3, L5) DSSCs were developed. For building glazing application, the essential criteria such as angular transmission, solar factor, and daylight glare index were determined by using theoretical equations and measured normal incident transmission. Average transmission and solar factor at normal incidence angle were found to be 53% and 0.57 for L2 DSSC, 50% and 0.55 for L3 DSSC, 37% and 0.39 for L5 DSSC. For vertical plane fenestration, angular transmission varies with varying incident angle. Using clearness index and glazing transmission correlation, one single yearly useable glazing transmission for different azimuthal direction was also evaluated for these DSSC type glazing. Finally, daylight glare analysis of DSSC glazing was carried out and compared with double glazing. For a clear sunny day, 21% glare can be reduced than double glazing using 37% transparent DSSC glazing. These analysis will help building engineers and architects to design a new low energy or retrofit building with DSSC glazing.

Acknowledgment

P. Selvaraj would like to acknowledge the College of Engineering, Mathematics and Physical Sciences, University of Exeter for the PhD fellowship. This work has been conducted as part of the research project 'Joint UK-India Clean Energy Centre (JUICE)' which is funded by the RCUK's Energy Programme (contract no: EP/P003605/1). The projects funders were not directly involved in the writing of this article. Dr Aritra Ghosh would like to acknowledge EPSRC IAA for its financial support to perform this work.

References

[1] Hans-Wilhelm, H. Schiffer, World Energy Resources | 2016, World Energy Counc, 2016, pp. 1–10. https://www.worldenergy.org/publications/2016/world-energy-resources-2016/. (Accessed 3 October 2018).
[2] U.S. Energy Information Administration. https://www.eia.gov/. (Accessed 3 October 2018).
[3] S. Nyquist, Energy 2050: Insights from the Ground up, McKinsey Co, 2016, pp. 1–3. https://www.mckinsey.com/industries/oil-and-gas/our-insights/energy-2050-insights-from-the-ground-up. (Accessed 3 October 2018).
[4] Organisation for Economic Co-operation and Development/International Energy Agency, International Energy Agency, 2017. https://www.iea.org/. (Accessed 3 October 2018).
[5] E. Halawa, A. Ghaffarianhoseini, A. Ghaffarianhoseini, J. Trombley, N. Hassan, M. Baig, S.Y. Yusoff, M. Azzam Ismail, A review on energy conscious designs of building façades in hot and humid climates: lessons for (and from) Kuala Lumpur and Darwin, Renew. Sustain. Energy Rev. 82 (2018) 2147–2161, https://doi.org/10.1016/j.rser.2017.08.061.
[6] M. Sudan, G.N. Tiwari, Energy matrices of the building by incorporating daylight concept for composite climate - an experimental study, J. Renew. Sustain. Energy 6 (2014), https://doi.org/10.1063/1.4898364.
[7] A. Ghosh, B. Norton, A. Duffy, Daylighting performance and glare calculation of a suspended particle device switchable glazing, Sol. Energy 132 (2016) 114–128. https://doi.org/10.1016/j.solener.2016.02.051.
[8] A. Ghosh, B. Norton, A. Duffy, Measured thermal & daylight performance of an evacuated glazing using an outdoor test cell, Appl. Energy 177 (2016) 196–203, https://doi.org/10.1016/j.apenergy.2016.05.118.
[9] A. Ghosh, B. Norton, Advances in switchable and highly insulating autonomous (self-powered) glazing systems for adaptive low energy buildings, Renew. Energy 126 (2018) 1003–1031, https://doi.org/10.1016/j.renene.2018.04.038.
[10] A. Ghosh, S. Sundaram, T.K. Mallick, Investigation of thermal and electrical performances of a combined semi- transparent PV-vacuum glazing, Appl. Energy 228 (2018) 1591–1600, https://doi.org/10.1016/j.apenergy.2018.07.040.
[11] A. Ghosh, S. Sundaram, T.K. Mallick, Colour properties and glazing factors evaluation of multicrystalline based semi-transparent Photovoltaic-vacuum glazing for BIPV application, Renew. Energy 131 (2019) 730–736, https://doi.org/10.1016/j.renene.2018.07.088.
[12] M. Saifullah, J. Gwak, J.H. Yun, Comprehensive review on material requirements, present status, and future prospects for building-integrated semitransparent photovoltaics (BISTPV), J. Mater. Chem. A. 4 (2016) 8512–8540, https://doi.org/10.1039/c6ta01016d.
[13] A.K. Shukla, K. Sudhakar, P. Baredar, A comprehensive review on design of building integrated photovoltaic system, Energy Build. 128 (2016) 99–110, https://doi.org/10.1016/j.enbuild.2016.06.077.
[14] E. Biyik, M. Araz, A. Hepbasli, M. Shahrestani, R. Yao, L. Shao, E. Essah, A.C. Oliveira, T. del Caño, E. Rico, J.L. Lechón, L. Andrade, A. Mendes, Y.B. Atlı, A key review of building integrated photovoltaic (BIPV) systems, Eng. Sci. Technol. Int. J. 20 (2017) 833–858, https://doi.org/10.1016/j.jestch.2017.01.009.
[15] B.P. Jelle, C. Breivik, H. Drolsum Røkenes, Building integrated photovoltaic products: a state-of-the-art review and future research opportunities, Sol. Energy Mater. Sol. Cells 100 (2012) 69–96, https://doi.org/10.1016/j.solmat.2011.12.016.
[16] N. Skandalos, D. Karamanis, PV glazing technologies, Renew. Sustain. Energy Rev. 49 (2015) 306–322, https://doi.org/10.1016/j.rser.2015.04.145.
[17] Y. Sun, K. Shanks, H. Baig, W. Zhang, X. Hao, Y. Li, B. He, R. Wilson, H. Liu, S. Sundaram, J. Zhang, L. Xie, T. Mallick, Y. Wu, Integrated CdTe PV glazing into windows: energy and daylight performance for different architecture designs, Appl. Energy (2018), https://doi.org/10.1016/j.apenergy.2018.09.133.
[18] M. Wang, J. Peng, N. Li, H. Yang, C. Wang, X. Li, T. Lu, Comparison of energy performance between PV double skin facades and PV insulating glass units, Appl. Energy 194 (2017) 148–160, https://doi.org/10.1016/j.apenergy.2017.03.019.
[19] S. Senthilarasu, S. Velumani, R. Sathyamoorthy, A. Subbarayan, J.A. Ascencio, G. Canizal, P.J. Sebastian, J.A. Chavez, R. Perez, Characterization of zinc phthalocyanine (ZnPc) for photovoltaic applications 389 (2003) 383–389, https://doi.org/10.1007/s00339-003-2184-7.
[20] T.D. Lee, A.U. Ebong, A review of thin film solar cell technologies and challenges, Renew. Sustain. Energy Rev. 70 (2017) 1286–1297, https://doi.org/10.1016/j.rser.2016.12.028.
[21] M. Saifullah, J. Gwak, J.H. Yun, Comprehensive review on material requirements, present status, and future prospects for building-integrated semitransparent photovoltaics (BISTPV), J. Mater. Chem. A. 4 (2016) 8512–8540, https://doi.org/10.1039/c6ta01016d.
[22] N. Skandalos, D. Karamanis, PV glazing technologies, Renew. Sustain. Energy Rev. 49 (2015) 306–322, https://doi.org/10.1016/j.rser.2015.04.145.

[23] E. Cuce, Toward multi-functional PV glazing technologies in low/zero carbon buildings: heat insulation solar glass - latest developments and future prospects, Renew. Sustain. Energy Rev. 60 (2016) 1286–1301, https://doi.org/10.1016/j.rser.2016.03.009.
[24] S.K. Anurag Roy, Parukuttaymma Sujatha Devi, S.S.D. Mamedov, Tapas Kumar Mallick, A Review on Applications of Cu2ZnSnS4 as Alternative Counter Electrodes in Dye- Sensitized Solar Cells, 2018, 070701, https://doi.org/10.1063/1.5038854.
[25] G. Richhariya, A. Kumar, P. Tekasakul, B. Gupta, Natural dyes for dye sensitized solar cell: a review, Renew. Sustain. Energy Rev. 69 (2017) 705–718, https://doi.org/10.1016/j.rser.2016.11.198.
[26] M.G. Kang, N.G. Park, Y.J. Park, K.S. Ryu, S.H. Chang, Manufacturing method for transparent electric windows using dye-sensitized TiO2 solar cells, Sol. Energy Mater. Sol. Cells 75 (2003) 475–479, https://doi.org/10.1016/S0927-0248(02)00202-7.
[27] J.G. Kang, J.H. Kim, J.T. Kim, Performance evaluation of DSC windows for buildings, Int. J. Photoenergy 2013 (2013), https://doi.org/10.1155/2013/472086.
[28] M. Morini, R. Corrao, Energy optimization of BIPV glass blocks: a multi-software study, Energy Procedia 111 (2017) 982–992, https://doi.org/10.1016/j.egypro.2017.03.261.
[29] A. Ghosh, P. Selvaraj, S. Sundaram, T.K. Mallick, The colour rendering index and correlated colour temperature of dye-sensitized solar cell for adaptive glazing application, Sol. Energy 163 (2018) 537–544, https://doi.org/10.1016/j.solener.2018.02.021.
[30] H.M. Lee, J.H. Yoon, Power performance analysis of a transparent DSSC BIPV window based on 2 year measurement data in a full-scale mock-up, Appl. Energy 225 (2018) 1013–1021, https://doi.org/10.1016/j.apenergy.2018.04.086.
[31] C. Cornaro, L. Renzi, M. Pierro, A. Di Carlo, A. Guglielmotti, Thermal and electrical characterization of a semi-transparent dye-sensitized photovoltaic module under real operating conditions, Energies 11 (2018), https://doi.org/10.3390/en11010155.
[32] P. Selvaraj, Anurag Roy, Habib Ullah, Parukuttyamma Sujatha Devi, Asif Ali Tahir, Tapas Kumar Mallick, Senthilarasu Sundaram, Soft - template synthesis of high surface area mesoporous titanium dioxide for dye - sensitized solar cells, Int. J. Energy Res. (2019) 523–534, https://doi.org/10.1002/er.4288.
[33] P. Selvaraj, H. Baig, T.K. Mallick, J. Siviter, A. Montecucco, W. Li, M. Paul, T. Sweet, M. Gao, A.R. Knox, S. Sundaram, Solar Energy Materials and Solar Cells Enhancing the efficiency of transparent dye-sensitized solar cells using concentrated light, Sol. Energy Mater. Sol. Cells 175 (2018) 29–34, https://doi.org/10.1016/j.solmat.2017.10.006.
[34] P. Selvaraj, H. Baig, T.K. Mallick, S. Sundaram, Charge transfer mechanics in transparent dye-sensitised solar cells under low concentration, Mater. Lett. (2018), https://doi.org/10.1016/j.matlet.2018.03.137.
[35] P.A. Waide, B. Norton, Variation of insolation transmission with glazing plane position and sky conditions, Trans. Am. Soc. Mech. Eng. J. Sol. Energy Eng. 125 (2003) 182–189, https://doi.org/10.1115/1.1563630.
[36] A. Ghosh, B. Norton, A. Duffy, Effect of atmospheric transmittance on performance of adaptive SPD-vacuum switchable glazing, Sol. Energy Mater. Sol. Cells 161 (2017) 424–431, https://doi.org/10.1016/j.solmat.2016.12.022.
[37] T.E. Kuhn, Calorimetric determination of the solar heat gain coefficient g with steady-state laboratory measurements, Energy Build. 84 (2014) 388–402, https://doi.org/10.1016/j.enbuild.2014.08.021.
[38] A. Ghosh, T.K. Mallick, Evaluation of optical properties and protection factors of a PDLC switchable glazing for low energy building integration, Sol. Energy Mater. Sol. Cells (2017) 0–1, https://doi.org/10.1016/j.solmat.2017.10.026.
[39] A. Ghosh, B. Norton, A. Duffy, Effect of sky conditions on light transmission through a suspended particle device switchable glazing, Sol. Energy Mater. Sol. Cells 160 (2017) 134–140, https://doi.org/10.1016/j.solmat.2016.09.049.
[40] A. Ghosh, B. Norton, T.K. Mallick, Daylight characteristics of a polymer dispersed liquid crystal switchable glazing, Sol. Energy Mater. Sol. Cells 174 (2018) 572–576, https://doi.org/10.1016/j.solmat.2017.09.047.
[41] E.S. Lee, D.L. DiBartolomeo, Application issues for large-area electrochromic windows in commercial buildings, Sol. Energy Mater. Sol. Cells 71 (2002) 465–491, https://doi.org/10.1016/S0927-0248(01)00101-5.
[42] M. Sudan, G.N. Tiwari, Daylighting and energy performance of a building for composite climate: an experimental study, Alexandria Eng. J. 55 (2016) 3091–3100, https://doi.org/10.1016/j.aej.2016.08.014.
[43] A. Thanachareonkit, J.L. Scartezzini, M. Andersen, Comparing daylighting performance assessment of buildings in scale models and test modules, Sol. Energy 79 (2005) 168–182, https://doi.org/10.1016/j.solener.2005.01.011.
[44] A. Ghosh, B. Norton, Durability of switching behaviour after outdoor exposure for a suspended particle device switchable glazing, Sol. Energy Mater. Sol. Cells 163 (2017) 178–184, https://doi.org/10.1016/j.solmat.2017.01.036.
[45] O. Bouvard, S. Vanzo, A. Schüler, Experimental determination of optical and thermal properties of semi-transparent photovoltaic modules based on dye-sensitized solar cells, Energy Procedia 78 (2015) 453–458, https://doi.org/10.1016/j.egypro.2015.11.696.